BIOCHEMISTRY
including biophysical chemistry & molecular biology

Article

pubs.acs.org/biochemistry

Crystal Structure of λ Exonuclease in Complex with DNA and Ca^{2+}

Jinjin Zhang,[†,‡,∥] Xinlei Pan,[†,‡] and Charles E. Bell*[,†,‡,§]

[†]Ohio State Biochemistry Program, [‡]Department of Molecular and Cellular Biochemistry, and [§]Department of Chemistry and Biochemistry, The Ohio State University, 1645 Neil Avenue, Columbus, Ohio 43210, United States

ABSTRACT: Bacteriophage λ exonuclease (λexo) is a ring-shaped homotrimer that resects double-stranded DNA ends in the 5′−3′ direction to generate a long 3′-overhang that is a substrate for recombination. λexo is a member of the type II restriction endonuclease-like superfamily of proteins that use a Mg^{2+}-dependent mechanism for nucleotide cleavage. A previous structure of λexo in complex with DNA and Mg^{2+} was determined using a nuclease defective K131A variant to trap a stable complex. This structure revealed the detailed coordination of the two active site Mg^{2+} ions but did not show the interactions involving the side chain of the conserved active site Lys-131 residue. Here, we have determined the crystal structure of wild-type (WT) λexo in complex with the same DNA substrate, but in the presence of Ca^{2+} instead of Mg^{2+}. Surprisingly, there is only one Ca^{2+} bound in the active site, near the position of Mg^{A} in the structure with Mg^{2+}. The scissile phosphate is displaced by 2.2 Å relative to its position in the structure with Mg^{2+}, and the network of interactions involving the attacking water molecule is broken. Thus, the structure does not represent a catalytic configuration. However, the crystal structure does show clear electron density for the side chain of Lys-131, which is held in place by interactions with Gln-157 and Glu-129. By combining the K131A−Mg^{2+} and WT−Ca^{2+} structures, we constructed a composite model to show the likely interactions of Lys-131 during catalysis. The implications with regard to the catalytic mechanism are discussed.

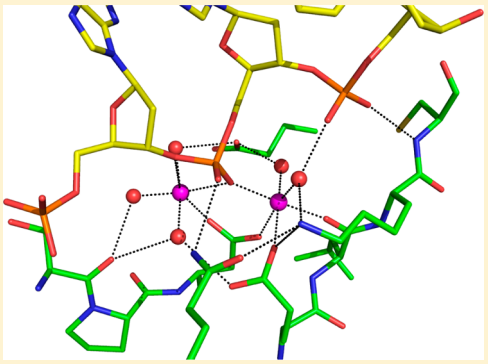

Bacteriophage λ exonuclease (λexo; M_r = 25.9 kDa; 226 amino acids) is an ATP-independent enzyme that binds to double-stranded DNA (dsDNA) ends and processively digests the 5′-strand into mononucleotides.[1,2] The reaction generates a long 3′-overhang that is a substrate for recombination.[3] Nuclease activity is metal-dependent, with a strong preference for Mg^{2+}, lower activity with Mn^{2+}, and no activity with Ca^{2+}.[3] The crystal structure of λexo revealed a toroidal homotrimer with a central funnel-shaped channel for tracking along the DNA.[4] The channel is wide enough to allow dsDNA to enter at one end but narrows at the other to allow passage of only single-stranded DNA (ssDNA). This led to a model for processivity in which the 3′-strand passes through the central hole on the trimer as the enzyme tracks along the DNA digesting the 5′-strand.[4]

The λexo monomer has a core α/β fold that is conserved in the "type II restriction endonuclease-like" (T2RE) superfamily of proteins,[5] which includes several type II restriction endonucleases[6,7] and a number of endo- and exonucleases involved in DNA repair,[8−12] recombination,[13−25] and RNA processing.[26−29] Version 1.75 of the SCOP database[30] includes 33 distinct T2RE proteins for which crystal structures have been determined. The core T2RE fold consists of a central five-stranded mixed β-sheet with an α-helix packed on either side. One of the α-helices is N-terminal, or "upstream" in the sequence, and the other is C-terminal, or "downstream". All of these enzymes contain a conserved PD-(D/E)XK signature motif (also called the DEK motif)[31,32] that is located on a pair of antiparallel β-strands. The motif contains two acidic residues that bind the metal ions and a third residue, usually lysine, that is also essential for catalysis. In addition, each of the two α-helices contributes a residue that is important for the reaction.

For many nuclease enzymes, including some with different folds, a common two-metal mechanism has been established, which involves an S_N2 displacement by an attacking water, inversion of configuration at the scissile phosphate, and generation of a 5′-phosphate and 3′-OH as products.[33−35] The site A metal binds and activates the attacking water; the site B metal binds a water that facilitates protonation of the leaving group, and both metals stabilize the negative charge and trigonal bipyramidal geometry of the transition state. Crystal structures of several T2RE family enzymes have revealed the expected two-metal geometry, with some variations, in the context of substrate,[8,23,36−40] product,[9,10,28,36,41,42] or inhibitor[43] complexes, or in the absence of ligand.[20,23,26] However, in other structures, there is only one metal bound,[44,45] or there is significant variation in the positions of the metals.[13,46−49] As a consequence, the precise roles of the metals and other active site residues are still being debated,[7,34,49−53] and there remains a need for detailed structural information for enzymes of this family in the presence of different metals.

Recently, we determined two crystal structures of λexo in complex with DNA.[40] One structure of the wild-type (WT) enzyme in the presence of Ca^{2+} used a blunt-ended symmetric

Received: September 12, 2014
Revised: November 4, 2014
Published: November 5, 2014

   dx.doi.org/10.1021/bi501155q | *Biochemistry* 2014, 53, 7415−7425

12 bp duplex with a 5′-OH at each end. This DNA bound to the central channel of the trimer as predicted but did not insert all the way into the active site, as the scissile phosphate was still ~10 Å from the single active site Ca^{2+} ion. The second structure used a K131A variant of the enzyme, which is completely inactive, to trap a stable enzyme−DNA complex in the presence of Mg^{2+}. The DNA in this structure was a 12 bp duplex with a two-nucleotide 5′-overhang on one end, which was designed to insert fully into the active site cleft. In addition, the 14-mer strand of the DNA was 5′-phosphorylated, because λexo requires a 5-phosphate for full activity. This structure revealed a complex that appears to be very close to a catalytic configuration, with the scissile phosphate bridging two active site Mg^{2+} ions, and the 5′-phosphate bound to a positively charged pocket at the end of the active site cleft.

As this latter structure was determined at 1.88 Å resolution,[40] it revealed the detailed coordination geometry of the two active site Mg^{2+} ions, including a water molecule bound to Mg^{A} that was suitably positioned for nucleophilic attack on the scissile phosphate. However, an important feature that was missing from this structure was the side chain of the highly conserved Lys-131 residue, because the K131A variant was used to trap the complex. Although the precise role of the catalytic lysine is unclear, on the basis of its position in related structures,[8,37−39,41,45] it is likely to bind and activate the attacking water molecule, possibly as a catalytic base to remove a proton.

To study the reaction mechanism of λexo in further detail, we have determined the structure of the WT enzyme in complex with the same DNA that was used for the structure of the K131A variant with Mg^{2+}, but in the presence of Ca^{2+} instead of Mg^{2+}, to prevent digestion. The DNA is bound in a very similar manner, but surprisingly, there is only one Ca^{2+} ion in the active site, instead of the two that were seen for Mg^{2+}. Consequently, the network of interactions involved in catalysis, including the attacking water molecule bound to Mg^{A}, is broken. However, the structure does show clear electron density for the position and interactions of the active site Lys-131 residue, from which we have constructed a composite model to assess the likely interactions of the lysine during catalysis. The relevance of this model for understanding the mechanism of the WT enzyme in the presence of Mg^{2+}, and for interpreting structures of related enzymes with varying numbers of metal ions, is discussed.

EXPERIMENTAL PROCEDURES

Protein Expression and Purification. λexo was expressed and purified as described previously.[40] Briefly, the protein was expressed in *Escherichia coli* BL21-AI cells from a pET14b vector as an N-terminal six-His fusion with a site for thrombin cleavage. The protein was purified by nickel affinity chromatography (GE Healthcare), thrombin cleavage to remove the six-His tag, a second nickel column to remove uncleaved protein, and anion exchange on HiTrap QHP (GE Healthcare). The final purified protein, which contains an extra N-terminal Gly-Ser-His sequence, was dialyzed into 20 mM Tris (pH 8.0) and 1 mM dithiothreitol (DTT), concentrated to ~20 mg/mL using a VivaSpin 20 device (Sartorius-Stedim Biotechnology), and frozen at −80 °C in small aliquots.

Exonuclease Assays. A 2686 bp *Pst*I-linearized pUC19 dsDNA substrate (NEB) was 3′-end-labeled with ^{32}P. Each 50 μL labeling reaction mixture contained 1× TdT buffer, 0.25 mM $CoCl_2$, 5.0 pmol of linear pUC19 DNA, 20 pmol of [α-^{32}P]ddATP, and 10 units of terminal transferase (NEB). The reaction mixture was incubated at 37 °C for 30 min, and the reaction was quenched by adding 10 μL of 0.2 M EDTA (pH 8.0). The labeled DNA was separated from reaction components by gel filtration on a G-25 MicroSpin column (GE Healthcare). For the exonuclease reactions (50 μL), the ^{32}P 3′-end-labeled dsDNA was incubated with λexo enzyme (0.05 or 0.5 nM trimer as indicated) at 37 °C in buffer containing 67 mM glycine-KOH (pH 9.4), 50 μg/mL bovine serum albumin, and varying concentrations of $MgCl_2$ and $CaCl_2$. Reactions were initiated by the addition of λexo enzyme after preincubation of all other reaction components. At the indicated time points, a 10 μL aliquot of the reaction mixture was removed, the reaction quenched by adding 1 μL of 0.25 M EDTA and 2 μL of BlueJuice loading dyes (Invitrogen), and the mixture analyzed by 0.8% agarose gel electrophoresis in TAE buffer. Dried gels were exposed using a Storm phosphorimager (GE Healthcare).

Crystallization and X-ray Data Collection. The DNA used for crystallization was prepared as described previously.[40] Briefly, two oligonucleotides, 5′-[P]AGCTACTGTACCGA-3′ and 5′-TCGGTACAGTAG-3′, were purchased in high-performance liquid chromatography-purified form from Integrated DNA Technologies, resuspended at 10 mM in ddH_2O, mixed in a 1:1 ratio, heated in a water bath to 90 °C, and slowly cooled to room temperature to allow annealing. For crystallization, 10 mg/mL purified λexo was mixed with a 1.2-fold molar excess of DNA in the presence of 5 mM $CaCl_2$, 20 mM Tris (pH 8.0), and 1 mM DTT. Crystals were grown by hanging drop vapor diffusion using a reservoir solution containing 23.4% PEG 3350, 0.3 M sodium acetate, and 0.1 M Tris (pH 9.5). Hanging drops were prepared by mixing 2 μL of the protein−DNA complex with 2 μL of reservoir solution. Crystals were gradually exchanged into a solution containing mother liquor with the level of PEG 3350 increased to 28%, mounted in nylon loops, and flash-frozen in liquid nitrogen. X-ray diffraction data were collected at a wavelength of 0.9793 Å at LRL-CAT beamline 31-ID of the Advanced Photon Source at Argonne National Laboratory (Argonne, IL). Diffraction data were integrated and scaled using MOSFLM and SCALA of the CCP4 suite.[54] On the basis of mean $I/\sigma I$ and R_{merge} criteria (Table 1), the diffraction data were truncated at 2.38 Å. Although the data extended to this resolution with mean $F/\sigma F$ values of >3.0 in all three reciprocal lattice directions, the data were moderately anisotropic. The exponential scale factors were −10.5 $Å^2$ for a^* and b^* and 21.0 $Å^2$ for c^*, giving a spread of 31.5 $Å^2$, as calculated using the UCLA Diffraction Anisotropy server.[54]

Structure Determination and Refinement. The crystal structure was determined by molecular replacement using the structure of the K131A variant of the λexo trimer determined previously in complex with DNA and Mg^{2+} [Protein Data Bank (PDB) entry 3SM4].[40] All atoms corresponding to solvent, including water molecules, phosphate, and Mg^{2+} ions, were excluded from the search model, so that it contained only atoms for protein and DNA. Molecular replacement using the MOLREP function in CCP4[55] and all of the diffraction data (to 2.38 Å resolution) led to a clear solution corresponding to a single trimer−DNA complex (contrast = 24.7) with initial R and R_{free} values of 43.1 and 42.9%, respectively. Rigid body refinement in REFMAC5,[55] treating the entire trimer−DNA complex as a single rigid body, reduced R and R_{free} to 39.5 and 39.3%, respectively. An initial round of restrained refinement without any NCS restraints reduced R and R_{free} to 27.2 and

Table 1. Data Collection and Refinement Statistics for the WT−Ca^{2+}−14/12-mer Complex[a]

Data Collection	
space group	*P*6(5)
cell dimensions [*a*, *b*, *c* (Å)]	80.0, 80.0, 241.6
resolution (Å)	40.0−2.38 (2.38−2.51)
R_{merge}	0.187 (0.644)
mean $I/\sigma I$	6.5 (3.2)
completeness (%)	99.9 (100.0)
redundancy	11.5 (11.6)
Refinement	
resolution (Å)	40.0−2.38
no. of reflections	33216
R_{work}/R_{free}	0.235/0.319
no. of atoms	
protein	5366
DNA	533
ligand/ion	13
water	236
B factor (Å^2)	
protein	29.7
DNA	42.7
ligand/ion	47.7
water	26.3
root-mean-square deviation	
bond lengths (Å)	0.017
bond angles (deg)	1.75

[a]The structure was refined using data collected from a single crystal. Numbers in parentheses are calculated for the highest-resolution shell only.

33.8%, respectively. Inclusion of NCS restraints of varying strengths led to an increase in *R* without a significant change in R_{free}, so NCS restraints were not included. After the initial round of refinement, clear electron density was observed for a single Ca^{2+} ion in each of the three active sites, each of the three Lys-131 side chains, two phosphate ions (in the two active sites to which the DNA was not bound), and several water molecules, all of which were added to the model using COOT.[56] Refinement of the model with all of these atoms included led to *R* and R_{free} values of 25.8 and 33.3%, respectively. Additional rounds of refinement and model building led to a final model comprised of three subunits of λexo, two strands of DNA (26 nucleotides), three Ca^{2+} ions, two phosphate ions, 236 water molecules, and final *R* and R_{free} values of 23.5 and 31.9%, respectively. An anisotropy-corrected data set was used for final stages of refinement.[54] Although this reduced the *R* and R_{free} values by only 0.07 and 0.17%, respectively, the electron density maps showed peaks for several additional water molecules, which were added to the model. Space group *P*6(5) has the potential for twinning, as was seen for the structure of the K131A λexo protein with DNA and Mg^{2+},[40] and the H-test indicated a small twinning fraction of 0.05 for this new crystal. However, use of the twin refinement option in REFMAC5 did not significantly reduce *R* or R_{free}, and was therefore not used. Data collection and refinement statistics are listed in Table 1. Figures were generated using PyMOL.[57] The atomic coordinates and structure factors have been deposited with the Protein Data Bank as entry 4WUZ.

RESULTS

Metal Dependence of λexo Activity. It was previously reported that λexo is most active in the presence of Mg^{2+}, 30% as active with Mn^{2+}, and inactive with Ca^{2+}, Cd^{2+}, Co^{2+}, Cu^{2+}, Fe^{2+}, Ni^{2+}, or Zn^{2+}.[3] The optimal Mg^{2+} concentration was between 1.0 and 2.5 mM.[3] Here, we have monitored digestion of a linear pUC19 dsDNA substrate to re-examine the dependence of λexo activity on Mg^{2+} concentration, as well as the activity in the presence of both Mg^{2+} and Ca^{2+} (Figure 1). As reported previously,[3] we observed that the activity of

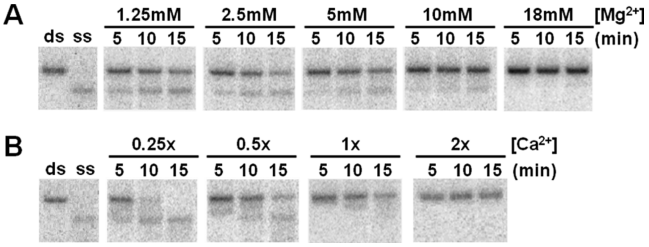

Figure 1. Metal dependence of λexo activity. The digestion of a ^{32}P 3′-end-labeled linear 2686 bp pUC19 dsDNA substrate (0.8 nM) was monitored by agarose gel electrophoresis, as described in Experimental Procedures. In each panel, the upper band shows the dsDNA substrate while the lower band shows the ssDNA product released when the opposing strand of the duplex is digested. Control reactions without enzyme are shown at left for the dsDNA substrate (ds) and ssDNA product (ss). The ssDNA control was prepared by heating half of the normal amount of dsDNA for 5 min at 95 °C and immediately placing it on ice. (A) Dependence of λexo activity on Mg^{2+} concentration. Notice that λexo activity is optimal at 1−2.5 mM Mg^{2+}, while higher concentrations of Mg^{2+} are inhibitory. (B) Dependence of λexo activity on Ca^{2+}, at the optimal Mg^{2+} concentration of 2.5 mM. Notice that the reaction is almost completely inhibited when Mg^{2+} and Ca^{2+} are present in equal amounts (1×). For the reactions in panel A, the concentration of λexo was 0.05 nM (16-fold excess of dsDNA substrate), whereas for panel B, 10-fold higher concentrations of λexo were used (0.5 nM trimer), to determine the point at which the inhibition by Ca^{2+} is complete.

λexo is optimal at Mg^{2+} concentrations ranging from 1.25 to 2.5 mM. λexo activity is significantly lower at 10 mM Mg^{2+} and dramatically lower at 18 mM Mg^{2+}. In the crystal structure of λexo determined at 5 mM Mg^{2+}, only two binding sites for Mg^{2+} were observed, the two in the active site to which the DNA was bound.[40] For several restriction endonucleases, inhibition of nuclease activity at higher than optimal concentrations of Mg^{2+} has been interpreted as evidence in favor of a one-metal mechanism in which Mg^{2+} bound to site A is required for catalysis, while Mg^{2+} bound at site B is inhibitory.[53] λexo is somewhat unique among T2RE enzymes in that it digests one nucleotide after another along the DNA in a highly processive reaction, instead of cleaving just once or twice for each molecule of substrate. Thus, the inhibition seen at Mg^{2+} concentrations of >10 mM for λexo could conceivably involve noncatalytic steps of the reaction cycle, such as release of mononucleotide product, or translocation along the DNA substrate. For example, if release of one or both of the Mg^{2+} ions is required for dissociation of the cleaved mononucleotide, then higher than optimal concentrations of Mg^{2+} could potentially slow the reaction by inhibiting product release.

We also determined the effect of varying concentrations of Ca^{2+} on λexo activity at the optimal Mg^{2+} concentration of 2.5 mM. These experiments were performed at 10-fold higher

dx.doi.org/10.1021/bi501155q | *Biochemistry* 2014, 53, 7415−7425

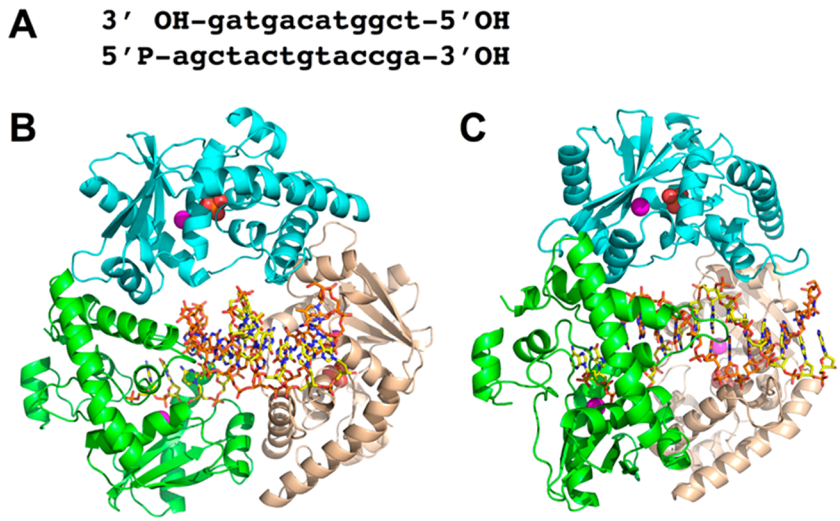

Figure 2. Structure of λexo in complex with DNA and Ca^{2+}. (A) Sequence of the DNA duplex used for crystallization. (B and C) Views of the λexo trimer looking down the 3-fold axis and rotated by ∼45° about the vertical axis, respectively. The λexo trimer is shown with subunit A colored cyan, subunit B colored green, and subunit C colored tan. The DNA is shown with the 14-mer strand colored yellow and the 12-mer strand colored orange. The 5′-phosphorylated two-nucleotide overhang of the 14-mer strand is inserted into the active site of the green subunit. A single Ca^{2+} ion, shown as a magenta sphere, is bound to the active site of each subunit. The two subunits without DNA in the active site contain bound phosphate ion, which is shown in CPK with red for oxygen and orange for phosphate.

concentrations of λexo, but still with a slight excess of substrate over enzyme, to determine the point at which inhibition of λexo activity is complete. As shown in Figure 1B, concentrations of Ca^{2+} as low as 1−2 times the concentration of Mg^{2+} completely inhibited λexo activity. This result is in contrast with the effect of Ca^{2+} on several restriction enzymes, where higher concentrations of Ca^{2+} (10−30 mM) increased the rate of cleavage.[53] The enhancement of cleavage was explained by a model in which high-affinity binding of Mg^{2+} to site A is required for catalytic activity, while lower-affinity binding of Ca^{2+} (but not Mg^{2+}) to site B enhances the affinity for the DNA substrate.[53] For λexo, structural data presented previously[40] and below indicate that Ca^{2+} binds to only one site on the protein (site A), both in the presence and in the absence of DNA. The crystallographic data show that, at least in the absence of DNA, Ca^{2+} binds to site A with an affinity higher than that of Mg^{2+}. This latter observation offers a possible explanation for the nearly complete inhibition seen at an only 1−2-fold excess of Ca^{2+} over Mg^{2+}.

X-ray Structure Determination. WT λexo was crystallized in complex with the 14/12-mer DNA diagrammed in Figure 2A in the presence of 5 mM $CaCl_2$. This is the same DNA that was used to crystallize the K131A variant in the presence of 5 mM $MgCl_2$.[40] A previous structure determined in the presence of 5 mM $CaCl_2$ used a 12/12-mer DNA that bound to the central channel of the trimer but did not insert fully into the active site. All three types of crystals grow under similar conditions and have the same space group and similar unit cell dimensions. There are small but significant changes in the unit cell dimensions, and molecular replacement was required to determine the structure for this study. It is interesting to note that the unit cell dimensions for the WT−Ca^{2+}−14/12 structure reported here are much closer to those of the WT−Ca^{2+}−12/12 structure (within 0.25%) than to those of the K131A−Mg^{2+}−14/12 structure (within 2.4%). This suggests that the unit cell differences are likely to be due to the metal ion (Ca^{2+} vs Mg^{2+}) or λexo version (WT vs K131A) as opposed to the DNA (12/12-mer vs 14/12-mer). After molecular replacement and an initial round of refinement with the DNA but no waters or solvent ions included in the model, the resulting maps showed clear electron density for each of the three Lys-131 side chains, three Ca^{2+} ions (one in each active site), and two phosphate ions (Figures 2B,C and 3A). As observed previously, the two phosphate ions bind in the two empty active sites (the two to which the DNA is not bound), to the same site as the terminal 5′-phosphate of the DNA. This observation re-emphasizes the point that phosphate must bind very tightly to this site, because phosphate was not present during the final anion exchange step of the purification, or in the final dialysis buffer or crystallization mixture.

The Active Site Contains a Single Ca^{2+} Ion Bound to Site A, with No Attacking Water Molecule. Surprisingly, in the active site to which the DNA is bound, there is only one Ca^{2+} ion, instead of the two that were seen for Mg^{2+} (Figure 3A). The single Ca^{2+} ion binds essentially at site A but is shifted slightly, by 1.0 Å toward site B (Figure 3C). There is clearly no peak in the electron density for a Ca^{2+} at site B. A few small peaks in the general vicinity of site B have been modeled as water molecules. The Ca^{2+} at site A is coordinated with near-octahedral geometry, by the pro-S_p oxygen of the scissile phosphate, the carboxylates of Asp-119 and Glu-129, the carbonyl oxygen of Leu-130, and a water molecule. The sixth coordination site, located behind the Ca^{2+} as seen in Figure 3A, is presumably occupied by a water molecule, although a peak for it was not seen in the electron density, presumably because of the limited (2.38 Å) resolution.

The coordination of the Ca^{2+} at site A is similar to what was observed for Mg^{A} in the structure with Mg^{2+} (Figure 3B),[40] with one notable exception. While the relative positions of Asp-119, Glu-129, and Leu-130 within the octahedral coordination sphere are the same for Ca^{2+} and Mg^{2+}, the positions of the scissile phosphate and the attacking water molecule are swapped in the structure with Ca^{2+}. This is due to the 1.0 Å shift in the position of the Ca^{2+} toward site B, combined with a 2.2 Å movement of the scissile phosphate upward, away from the active site (Figure 3C). The distance of 3.3 Å between the

dx.doi.org/10.1021/bi501155q | Biochemistry 2014, 53, 7415−7425

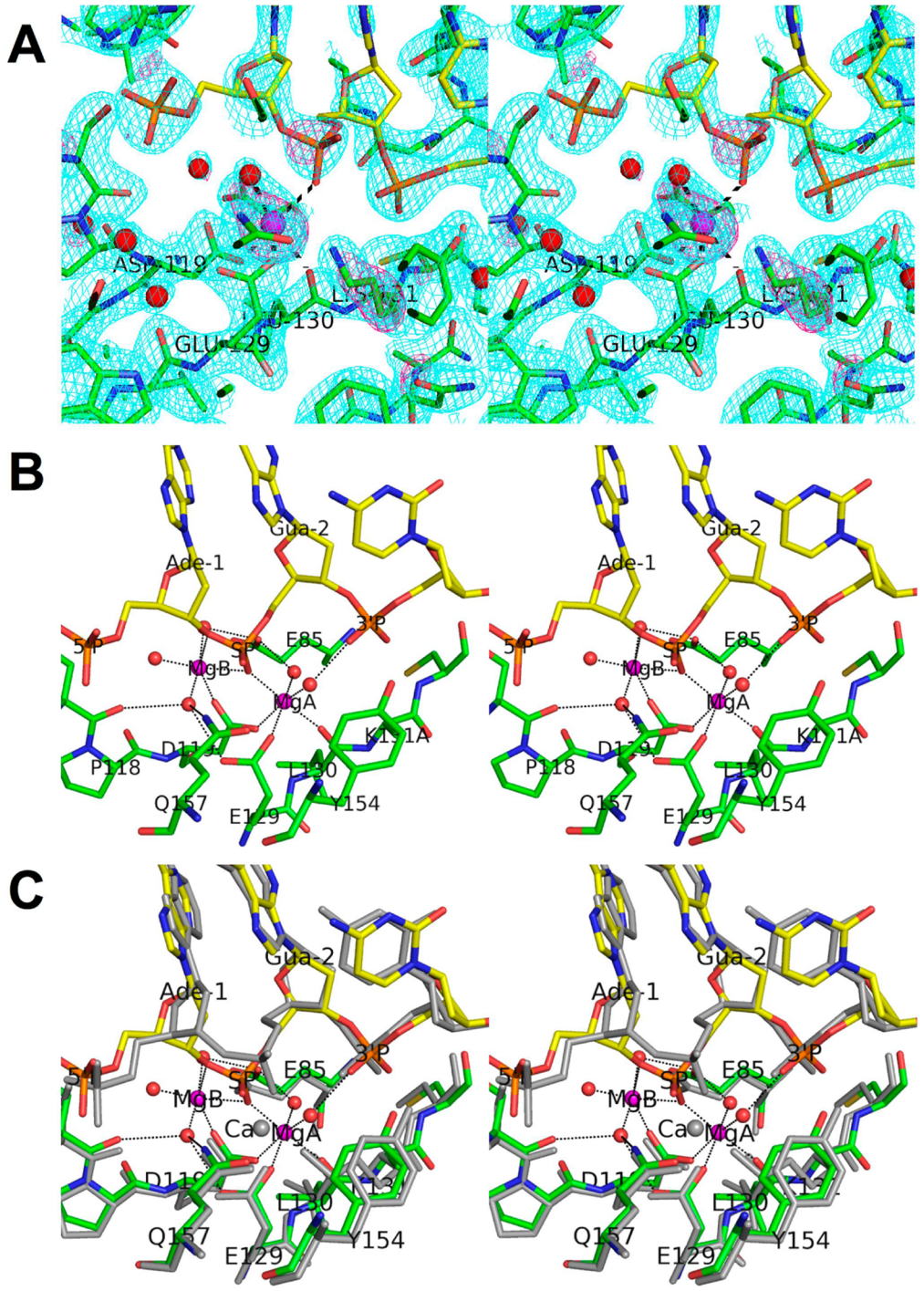

Figure 3. Comparison of the active site interactions with Ca^{2+} and Mg^{2+}. (A) Active site electron density for the structure with Ca^{2+}. The blue cage shows a $2F_o - F_c$ map calculated at 2.38 Å resolution with phases from the final model and contoured at 2σ. The pink cage shows the $F_o - F_c$ map contoured at 3σ with phases calculated before the Ca^{2+} and the Lys-131 side chain model were added. As shown by the dashed lines, the single Ca^{2+} ion is coordinated by the scissile phosphate, the carboxylates of Asp-119 and Glu-129, the backbone carbonyl of Leu-130, and a water molecule. (B) Active site of the K131A variant with DNA and Mg^{2+} (PDB entry 3SM4).[40] The two Mg^{2+} ions are bridged by the scissile phosphate (labeled SP) and the carboxylate of Asp-119. Dashed lines show the interactions of the metals and the liganding water molecules. (C) Overlay of the structures with Ca^{2+} (gray) and Mg^{2+} (green bonds for protein and yellow for DNA). Dashed lines are from the structure with Mg^{2+}. Notice that the Ca^{2+} is close to Mg^{A} but shifted by 1.0 Å toward Mg^{B}. Also notice the upward displacement of the scissile phosphate in the structure with Ca^{2+}.

scissile phosphate and the Ca^{2+} is considerably longer than the corresponding distances of 2.0 Å seen for Mg^{2+}. The net result is that there is no water molecule on the Ca^{2+} that is appropriately positioned for in-line attack on the scissile phosphate. Altogether, because of the absence of a metal at site B, the 1.0 Å shift in the position of the Ca^{2+} at site A, and the 2.2 Å upward movement of the scissile phosphate, the network of interactions seen in the structure with Mg^{2+} that was close to a catalytic configuration is substantially broken in the structure with Ca^{2+}.

Interactions of the Conserved Active Site Lysine Residue, Lys-131. In the new structure, there is clear electron

dx.doi.org/10.1021/bi501155q | *Biochemistry* 2014, 53, 7415−7425

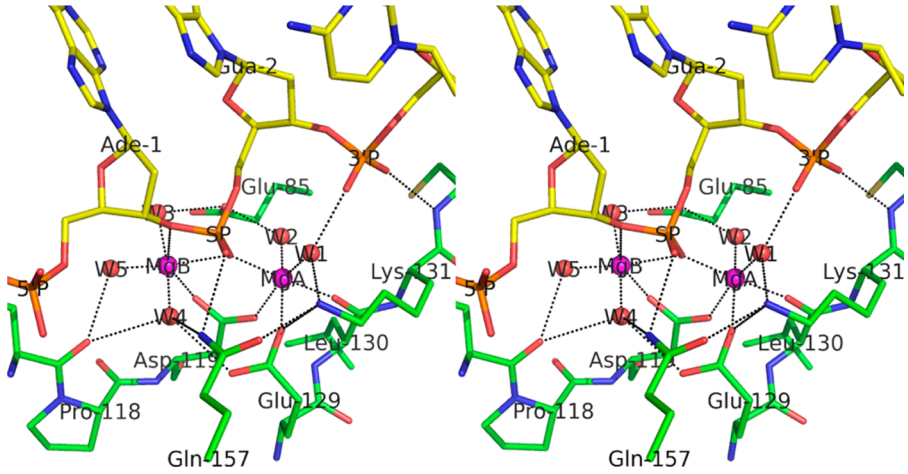

Figure 4. Composite model showing the likely position of the catalytic lysine (Lys-131) in the complex with DNA and Mg^{2+}. The composite model contains the atoms from the K131A–DNA–Mg^{2+} structure (PDB entry 3SM4),[40] but with the side chain of Lys-131 from the structure with DNA and Ca^{2+} determined here grafted on. Interactions of the metals, the liganding waters, and key active site residues are shown as dotted lines. The scissile phosphate and the phosphates 5′ and 3′ to it are labeled SP, 5′-P, and 3′-P, respectively. Notice that Lys-131 forms hydrogen bonds with Gln-157, Glu-129, and the attacking water (W1). Also notice the approximate tetrahedral arrangement of the pro-R_p atom of the 3′-phosphate, the amine group of Lys-131, Mg^A, and the phosphorus atom of the scissile phosphate, around the attacking water molecule. The pro-S_p oxygen of the scissile phosphate bridges the two metal ions, while the pro-R_p oxygen hydrogen bonds to Gln-157.

density for the side chain of Lys-131 (Figure 3A), which was not seen in the structure with Mg^{2+} due to the use of the K131A variant. The side chain of Lys-131 extends into the active site to form ion pairs with the pro-S_p atom of the scissile phosphate (2.9 Å) and the OE2 atom of Glu-129 (2.9 Å). It also forms a hydrogen bond with the OE1 atom of Gln-157 (2.8 Å), a conserved residue from the downstream α-helix that also hydrogen bonds to the scissile phosphate (Figure 3C). Lys-131 also forms a long-range ion pair (3.9 Å) with the pro-R_p atom of the neighboring 3′-phosphate. The network of interactions involving Lys-131 is partially shielded from solvent by the side chain of Tyr-154, another conserved residue from the downstream α-helix, which closes over the active site and forms a hydrogen bond with one of the phosphates. Interestingly, in the K131A–Mg^{2+} structure determined previously,[40] the aromatic ring of Tyr-154 is shifted inward by 2.0 Å, apparently to fill the cavity left by the absence of the Lys-131 side chain (Figure 3C).

A putative role of the active site lysine is to bind and somehow activate the attacking water molecule. Thus, in determining the structure of the WT enzyme with Ca^{2+}, we were hoping to visualize this interaction. In the structure, however, there is no water molecule bound to the Ca^{2+} that would correspond to the putative hydrolytic water seen in the structure with Mg^{2+}. Thus, to assess the possible interactions of Lys-131 that would occur in the presence of Mg^{2+}, we have constructed a composite model by grafting the side chain of Lys-131 from the structure with Ca^{2+} onto the structure with Mg^{2+} (Figure 4). This model is likely to be reasonably accurate, because the Cα and Cβ atoms of Lys- and Ala-131 from the two structures align within 0.29 Å of one another. In the composite model, the terminal amine of Lys-131 is indeed positioned 2.7 Å from the hydrolytic water molecule, which is labeled "W1" in Figure 4. It also forms the same hydrogen bonding interactions with Glu-129 and Gln-157 that are seen in the structure with Ca^{2+} (Figure 3C).

The composite model suggests that Lys-131 is likely to be farther from the scissile phosphate than one might expect from the structure with Ca^{2+}: it is 2.9 Å from the pro-S_p atom of the scissile phosphate in the structure with Ca^{2+} and 3.5 Å from the pro-R_p atom in the composite model. This difference is mainly due to the 2.2 Å shift in the position of the scissile phosphate in the Ca^{2+} structure. Lys-131 is ∼4 Å from the neighboring 3′-phosphate in both structures. The implications of these interactions with regard to the catalytic mechanism will be discussed.

DISCUSSION

λexo is a member of a large superfamily of Mg^{2+}-dependent nuclease enzymes that share a common core fold and a PD-(D/E)XK active site signature motif. Members of this superfamily catalyze endo- or exonucleolytic reactions on DNA or RNA substrates. While the structures of considerably more than 30 proteins of this superfamily have been determined, relatively few of them have been determined in the presence of the nucleic acid substrate (or product) and the appropriate metal ion.[8−10,13,24,28,36−49] Of these, many structures reveal only one metal ion instead of two at the active site,[44,45] or metal–ligand geometries that otherwise deviate from the canonical two-metal mechanism originally proposed for the proofreading domain of DNA polymerase I.[13,46−49] The observed deviations could reflect true differences in the catalytic mechanism, but given the common evolutionary origin and conserved active site, it seems more likely that the differences arise from the necessity of altering the complex in some manner to prevent turnover. Because of the lack of a firm consensus for the structure of the ground state complex of these enzymes, there is still much debate about the catalytic mechanism, in particular with regard to the number and roles of the metal ions, the role of the catalytic lysine, and the role of the 3′-phosphate.[7,34,49−53,58−60]

Our previous structure of the K131A mutant of λexo in complex with DNA and Mg^{2+} revealed a two-metal active site that appears to be very close to the canonical two-metal geometry.[33,34,40] It is one of the few structures of a PD-(D/E)XK enzyme that has been determined in a ground state complex with Mg^{2+}, as opposed to Ca^{2+} or Mn^{2+}. This was possible for λexo because of the complete inactivity of the K131A mutant. By several criteria, the K131A–Mg^{2+} structure

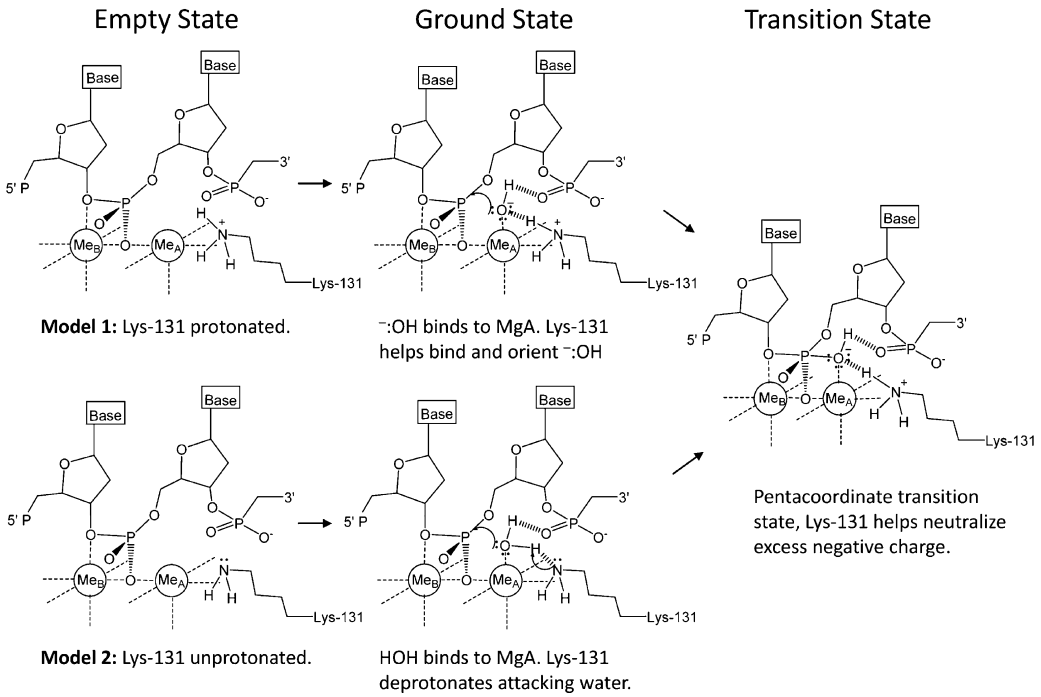

Figure 5. Two models for the reaction mechanism of λ exonuclease. In model 1 (top) the "empty" state shown at the left has Lys-131 in its protonated (charged) state, which selects for binding of a hydroxide ion, as opposed to a water molecule, at the attacking position on Mg^A. In model 2 (bottom), the "empty" state has Lys-131 in its unprotonated (neutral) state, which provides an ideal binding site for a water molecule at the attacking position on Mg^A. In model 2, Lys-131 acts as a general base to deprotonate the attacking water, whereas in model 1, Lys-131 selects for binding of a hydroxide. Both models show the pro-R_p oxygen of the 3′-phosphate accepting a hydrogen bond from the attacking water or hydroxide, to bind and orient it further.

appears to be as close to having the probable geometry of the transition state as any structure of a member of this family. These criteria include a short distance of 4.0 Å between the two Mg^{2+} ions, near-octahedral coordination geometry for the metals, metal−ligand distances ranging from 2.2 to 2.4 Å that are ideal for Mg^{2+}, a short distance of 3.2 Å between the attacking water and the phosphorus atom of the scissile phosphate, and a nearly linear arrangement of the scissile phosphorus atom with the attacking and leaving oxygen atoms (the O−P−O angle is 171°). This structure thus appears to provide a particularly good framework for analysis of the catalytic mechanism. Structures with near-canonical two-metal geometry have also been determined for *Mut*H,[8] *Bam*HI,[36] *Bgl*I,[37] *Mva*I,[38] and *Bcn*I.[39] Interestingly, the active sites of λexo and *Bgl*I in particular are strikingly similar to one another, despite the fact that the two proteins share only very limited sequence similarity with one another.

A key feature that is missing from the K131A−Mg^{2+} structure is the interactions involving the catalytic lysine, which was truncated to alanine to trap the complex. On the basis of structures of related enzymes,[8,45] several possible roles for the equivalent lysine have been suggested, including stabilization of the excess negative charge on the scissile phosphate that builds up in the transition state, activation of the attacking water by orienting it via hydrogen bond formation, or more direct activation of the attacking water by acting as a catalytic base to abstract a proton.[8,45] To assess the catalytic role of Lys-131 of λexo, the goal of this study was to visualize the interactions of Lys-131 in the context of a functional active site, by determining the structure of the WT enzyme in complex with DNA in the presence of Ca^{2+}. For most T2RE enzymes, Ca^{2+} can functionally replace Mg^{2+} for substrate binding but does not facilitate cleavage. Structures of several T2RE enzymes determined in the presence of nucleic acid substrate and Ca^{2+} show two-site binding with the near-octahedral geometry expected for Mg^{2+}, albeit with slightly longer coordination distances, because of the larger atomic radius of Ca^{2+}.[8,36−39]

Surprisingly, in the structure of λexo with DNA and Ca^{2+} determined here, there is only one Ca^{2+} in the active site, instead of the two that were seen for Mg^{2+}, despite the fact that the two complexes crystallize under nearly identical conditions and with very similar unit cell dimensions. The single metal ion binds very close to site A but is shifted by ∼1 Å toward site B, possibly because of its larger atomic radius. Presumably, this shift of the site A Ca^{2+} toward site B is what prevents the binding of the second Ca^{2+} ion to site B. The Ca^{2+} at site A is coordinated by the same ligands as Mg^A in the K131A−Mg^{2+} structure, but with one major difference. Because of a 2.2 Å upward movement of the scissile phosphate, the positions of the water molecule and the pro-S_p atom of the scissile phosphate on the coordination sphere of the Ca^{2+} are interchanged. As a result, there is no water molecule bound to the Ca^{2+} that is suitably positioned for in-line attack on the phosphate, and the network of interactions that is poised for catalysis in the structure with Mg^{2+} is broken. Interestingly, similar modes of coordination of a single Ca^{2+} in a noncatalytic configuration have been observed for other T2RE enzymes, such as DXO ribonuclease (PDB entry 4J7M)[28] and *Eco*RI (PDB entry 1QPS).[47]

Although the structure with Ca^{2+} does not reveal the interactions of the catalytic lysine with the hydrolytic water molecule as we had intended, it does show clear electron density for the Lys-131 side chain, which forms short hydrogen bonds with the side chains of Gln-157 and Glu-129. The WT−

dx.doi.org/10.1021/bi501155q | *Biochemistry* 2014, 53, 7415−7425

Ca^{2+} structure thus permits us to build a composite model by grafting the atoms of the Lys-131 side chain from the WT−Ca^{2+} structure onto the K131A−Mg^{2+} structure, as shown in Figure 4. Because Lys-131 is relatively fixed in place by its interactions with Gln-157 and Glu-129, the composite model is likely to be close to the true ground state and is thus likely to show the interactions of Lys-131 with the other groups in the active site that are relevant to catalysis, such as the attacking water and the scissile phosphate.

Examination of the composite model reveals several interesting features. First and foremost, the terminal amine group of Lys-131 is 2.7 Å from the attacking water and could thus form a stabilizing hydrogen bond with it. Second, in addition to the interactions with Gln-157 and Glu-129, Lys-131 is within 3.5 Å of the pro-S_p atom of the scissile phosphate. This distance is likely to be even shorter in the transition state, in which the two metals are expected to move closer together. Thus, Lys-131 could help to stabilize the excess negative charge on the scissile phosphate in the transition state by direct ion pair formation. Third, the geometry of the interacting groups around the attacking water molecule, including Lys-131, Mg^A, the pro-S_p oxygen of the 3′-phosphate, and the phosphorus atom of the scissile phosphate, is approximately tetrahedral. This geometry would be even closer to tetrahedral if the attacking water were to move closer to the phosphorus, as expected for the transition state. A similar tetrahedral arrangement of the equivalent groups around the attacking water has been seen in the structures of several other T2RE enzymes,[8,37−39,45] and it thus appears to be a conserved feature that is fundamental to catalysis.

Fourth, via examination of the network of hydrogen bonding interactions in the active site, it appears that in the ground state, either the attacking water or Lys-131 must be deprotonated. Of the three potential hydrogen atoms on the terminal amine of Lys-131, two must point toward lone pairs of electrons on the oxygen atoms of Gln-157 and Glu-129, to donate hydrogen bonds. The third hydrogen, if present, would point toward the hydrolytic water molecule (Figure 4). The attacking water would presumably have its two lone pairs facing Mg^A and the scissile phosphate, and one of its hydrogens facing the pro-R_p atom of the 3′-phosphate. The second hydrogen, if present, would face the amine group of Lys-131. Thus, if the attacking water and Lys-131 are to interact favorably, one of them must be deprotonated.

Proposed Mechanism of Cleavage. On the basis of this structural framework, we envision two possible models for the chemical step of DNA cleavage by λexo (Figure 5). The two models differ only in the way in which the hydroxide nucleophile is generated in the initial stages of the reaction. In the first model, the enzyme−DNA complex, with two Mg^{2+} ions bridging the scissile phosphate, and Lys-131 in its protonated, positively charged state, presents an ideal and selective binding site on Mg^A for a negatively charged hydroxide ion. Binding of the hydroxide over the water is favored not only by the positive charges on Mg^A and protonated Lys-131 but also by the projection of a tetrahedral pattern of interacting groups that favors the three lone pairs and one hydrogen of the hydroxide. Binding of the water, with two hydrogens, is excluded if Lys-131 is protonated. Once a hydroxide ion is bound and oriented on Mg^A, it attacks the scissile phosphate to form the pentacoordinate transition state, which has a net charge of −2. The excess negative charge on the phosphate is stabilized in part by the two metal ions, which symmetrically coordinate the pro-S_p oxygen of the scissile phosphate, the attacking water, and the O3′ leaving group, and also in part by Lys-131 and Gln-157, which form an ion pair with and donate a hydrogen bond to the pro-R_p atom of the scissile phosphate, respectively. On the downhill side of the reaction, protonation of the O3′ leaving group could be facilitated by one of the three water molecules bound to Mg^B. Wat-3 (as labeled in Figure 4) is 3.4 Å from the O3′ atom of the scissile phosphate and is a likely candidate that could be further activated by its interaction with Glu-85, a conserved residue from the upstream α-helix that forms outer sphere coordination to both metals via liganding water molecules. Another candidate, Wat-4, is 3.1 Å from the O3′ atom and forms hydrogen bonds with Glu-129 (an Mg^A ligand) and the backbone carbonyl of Ser-117, the residue preceding the proline of the PD-(D/E)XK motif.

Model 2 differs from model 1 only in the way in which the attacking nucleophile is generated. In model 2, the enzyme−DNA complex, with two Mg^{2+} ions bridging the scissile phosphate, and Lys-131 in its neutral, unprotonated state, forms a binding site for a water molecule at the attacking position on Mg^A. The water donates its two hydrogen atoms to form hydrogen bonds with the lone pair on the Lys-131 amino group and the pro-S_p oxygen of the 3′- phosphate and projects its two lone pairs toward Mg^A and the phosphorus of the scissile phosphate. Lys-131 acts as a catalytic base to abstract a proton from the water molecule, to form the more nucleophilic hydroxide, which is then poised to attack the scissile phosphate. Lys-131, now in the positively charged, protonated state, is poised to donate a hydrogen bond to and electrostatically stabilize the negative charge on the pro-R_p atom of the scissile phosphate in the transition state.

Determination of which of these two models is more likely to be correct depends on the pK_a values of Lys-131 and of the attacking water in the context of the active site. On the basis of the intrinsic pK_a values of 10.0 and 15.7 for the lysine and the water molecule, respectively, the lysine would be ∼1 million times more likely to be deprotonated in solution at the optimal pH of the reaction, which is 9.2−9.5.[1] However, a water molecule bound to a Mg^{2+} ion would have its pK_a reduced significantly, to around 11.5. How is the pK_a of the lysine likely to be altered from its intrinsic value, based on its interactions in the active site? In the composite model, Lys-131 is within 4 Å of at least four atoms bearing a full or partial negative charge, including the pro-R_p oxygen of the scissile phosphate (3.5 Å), OE2 of Glu-129 (2.8 Å), OE1 of Gln-157 (2.8 Å), and the pro-R_p oxygen of the 3′-phosphate (4.1 Å). It is also within 2.7 Å of the hydrolytic water molecule (or hydroxide ion) and 4.0 Å of Mg^A. Lys-131 is at least partially buried by interactions with the phenyl rings of Tyr-154 and Phe-172, which would tend to strengthen any electrostatic interactions. In summary, because Lys-131 is partially buried and juxtaposed to significantly more negative than positive charge, it is likely that its pK_a would be elevated relative to the intrinsic value of 10.0, but the extent is difficult to determine. On the basis of this analysis, it appears that the pK_a values of Lys-131 and the attacking water are likely to be similar, making it difficult to judge which of the two models is more likely to be correct.

While the great majority of PD-(D/E)XK enzymes have a lysine at the position corresponding to Lys-131 of λexo, in a few cases, most notably *Bam*HI[36] and *Bgl*II,[44] the catalytic lysine is replaced with glutamate and glutamine, respectively. As discussed previously,[8,34,45] while a glutamate could function as a

catalytic base in a manner similar to that of a lysine, provided that the local environment were to elevate its pK_a from the intrinsic value of 4.4, clearly a glutamine could not. The amide of the glutamine side chain could however function as a hydrogen bond donor, to help select for binding of a hydroxide at Mg^A instead of a water molecule, as proposed in model 1. Thus, if a strictly conserved mechanism for the chemical step is employed by all members of the PD-(D/E)XK superfamily, the fact that the catalytic lysine can be replaced with a glutamine in a related enzyme would tend to favor model 1.

For *Eco*RI, *Eco*RV, and other restriction endonucleases, the neighboring 3′-phosphate of the DNA substrate itself has been proposed to be the catalytic base that removes the proton from the attacking water molecule.[58−60] This suggestion was based on structural considerations of *Eco*RI and *Eco*RV showing that a water molecule bound to the 3′-phosphate would be in position for in-line attack on the scissile phosphate,[59] and on experiments measuring the effects of methylphosphonate or phorphothioate modifications to the 3′-phosphate on the rate of cleavage.[59−62] As described above, in λexo the pro-R_p atom of the 3′-phosphate indeed forms a short hydrogen bond (2.5 Å) with the attacking water (Figure 4). The other nonbridging oxygen of the 3′-phosphate, pro-S_p, accepts a hydrogen bond (2.8 Å) from the backbone amide of Cys-132, the residue that follows the catalytic lysine. Similar interactions of the 3′-phosphate with the attacking water and the equivalent backbone amide have been seen in several other T2RE enzymes.[8,37−39,45]

As has been noted previously,[45] a key argument against the 3′-phosphate acting as a catalytic base to abstract a proton from the attacking water is its low intrinsic pK_a of 2.2. This mechanism seems particularly unlikely for λexo, for which the optimal pH is 9.2−9.5,[3] which is within 0.5−0.8 unit of the intrinsic pK_a of 10.0 for lysine, but 7 full units from the intrinsic pK_a of the 3′-phosphate. Moreover, there do not appear to be any negatively charged or apolar groups in contact with the 3′-phosphate that would potentially increase its pK_a to increase its affinity for protons. In fact, the hydrogen bond formed by the pro-S_p atom of the 3′-phosphate with the backbone amide of Cys-132 would tend to decrease the potential for the pro-R_p oxygen to accept a proton. Thus, for λexo, it seems that if there is a catalytic base, it is far more likely to be the amine group of Lys-131 than the 3′-phosphate. We suggest that the 3′-phosphate, together with the backbone amide of Cys-132, helps to form a tight network of hydrogen bonds to bind and orient the attacking water (or hydroxide ion) at the correct position on Mg^A. If it is a water molecule that initially binds to Mg^A, then Lys-131, in its deprotonated state, is likely to act as the catalytic base.

CONCLUSIONS

We have determined the crystal structure of WT λexo in complex with DNA and Ca^{2+}, to assess the interactions of the catalytic lysine residue, Lys-131, which was truncated to alanine in the previously determined structure with DNA and Mg^{2+}. Surprisingly, Ca^{2+} binds to only one site on the enzyme (site A), and in a noncatalytic configuration, with no attacking water molecule. The structure is reminiscent of previous structures of related enzymes, such as *Eco*RI, *Eco*RV, *Pvu*II, *Hinc*II, and DXO ribonuclease, in which the metals are bound in sites that deviate from the canonical two-metal mechanism. Given that the previous structure of λexo with DNA and Mg^{2+} revealed the standard two-metal geometry, the new structure with Ca^{2+} provides more evidence in favor of the argument that the noncanonical metal binding positions are likely to arise from the need to alter the complex for crystallization, as opposed to different catalytic mechanisms. Although the structure with DNA and Ca^{2+} does not reveal a catalytic configuration, it does show the position of the catalytic Lys-131 side chain, which permits the construction of a composite model, to assess the likely interactions of Lys-131 with the other groups in the active site during catalysis. The structural data favor a mechanism in which Lys-131 either helps to select for binding of a hydroxide ion at Mg^A for attack on the scissile phosphate or acts as a catalytic base to deprotonate the attacking water.

AUTHOR INFORMATION

Corresponding Author

*E-mail: bell.489@osu.edu. Telephone: (614) 688-3115.

Present Address

[‖]J.Z.: Infectious Disease Division, NewLink Genetics Corp., 2503 S. Loop Dr., Suite 5100, Ames, IA 50010.

Author Contributions

J.Z. and X.P. contributed equally to this work.

Funding

This work was funded by Grant MCB-1021966 (to C.E.B.) from the National Science Foundation.

Notes

The authors declare no competing financial interest.

ACKNOWLEDGMENTS

We thank Dr. Jimmy Cowan and Dr. Dehua Pei for comments on the manuscript. This research used resources of the Advanced Photon Source, a U.S. Department of Energy (DOE) Office of Science User Facility operated for the DOE Office of Science by Argonne National Laboratory under Contract DE-AC02-06CH11357.

REFERENCES

(1) Little, J. W. (1967) An exonuclease induced by bacteriophage lambda II. Nature of the enzymatic reaction. *J. Biol. Chem. 242*, 679−686.

(2) Carter, D. M., and Radding, C. M. (1971) The role of exonuclease and β protein of phage λ in genetic recombination. II. Substrate specificity and the mode of action of λ exonuclease. *J. Biol. Chem. 246*, 2502−2512.

(3) Little, J. W., Lehman, I. R., and Kaiser, A. D. (1967) An exonuclease induced by bacteriophage λ. I. Preparation of the crystalline enzyme. *J. Biol. Chem. 242*, 672−678.

(4) Kovall, R., and Matthews, B. W. (1997) Toroidal structure of lambda-exonuclease. *Science 277*, 1824−1827.

(5) Kovall, R. A., and Matthews, B. W. (1998) Structural, functional, and evolutionary relationships between λ-exonuclease and the type II restriction endonucleases. *Proc. Natl. Acad. Sci. U.S.A. 95*, 7893−7897.

(6) Kovall, R. A., and Matthews, B. W. (1999) Type II restriction endonucleases: Structural, functional, and evolutionary relationships. *Curr. Opin. Chem. Biol. 3*, 578−583.

(7) Pingoud, A., Fuxreiter, M., Pingoud, V., and Wende, W. (2005) Type II restriction endonucleases: Structure and mechanism. *Cell. Mol. Life Sci. 62*, 685−707.

(8) Lee, J. Y., Chang, J., Joseph, N., Ghirlando, R., Rao, D. N., and Yang, W. (2005) MutH complexed with hemi- and unmethylated DNAs: Coupling base recognition and DNA cleavage. *Mol. Cell 20*, 155−166.

(9) Tsutakawa, S. E., Jingami, H., and Morikawa, K. (1999) Recognition of a TG mismatch: The crystal structure of very short

patch repair endonuclease in complex with a DNA duplex. *Cell 99*, 615−623.
(10) Bunting, K. A., Roe, S. M., Headley, A., Brown, T., Savva, R., and Pearl, L. H. (2003) Crystal structure of the *Escherichia coli* dcm very-short-patch DNA repair endonuclease bound to its reaction product-site in a DNA superhelix. *Nucleic Acids Res. 31*, 1633−1639.
(11) Singleton, M. R., Dillingham, M. S., Gaudier, M., Kowalczykowski, S. C., and Wigley, D. B. (2004) Crystal structure of RecBCD enzyme reveals a machine for processing DNA breaks. *Nature 432*, 187−193.
(12) Krajewski, W. W., Fu, X., Wilkinson, M., Cronin, N. B., Dillingham, M. S., and Wigley, D. B. (2014) Structural basis for translocation by AddAB helicase-nuclease and its arrest at χ sites. *Nature 17*, 416−419.
(13) Yang, W., Chen, W.-Y., Want, H., Ho, J. W. S., Huang, J.-D., et al. (2011) Structural and functional insight into the mechanism of an alkaline exonuclease from *Laribacter hongkogenesis*. *Nucleic Acids Res. 39*, 9803−9819.
(14) Zhang, J., Xing, X., Herr, A. B., and Bell, C. E. (2009) Crystal structure of *E. coli* RecE protein reveals a toroidal tetramer for processing double-stranded DNA breaks. *Structure 17*, 690−702.
(15) Bagnéris, C., Briggs, L. C., Savva, R., Ebrahimi, B., and Barrett, T. E. (2011) Crystal structure of a KSHV-SOX-DNA complex: Insights into the molecular mechanisms underlying DNase activity and host shutoff. *Nucleic Acids Res. 39*, 5744−5756.
(16) Dahlroth, S. L., Gurmu, D., Haas, J., Erlandsen, H., and Nordlund, P. (2009) Crystal structure of the shutoff and exonuclease protein from oncogenic Kaposi's sarcoma-associated herpes virus. *FEBS J. 276*, 6636−6645.
(17) Buisson, M., et al. (2006) A bridge crosses the active-site canyon of the Epstein-Barr virus nuclease with DNase and RNase activities. *J. Mol. Biol. 391*, 717−728.
(18) Newman, M., Murray-Rust, J., Lally, J., Rudolf, J., Fadden, A., Knowles, P. P., White, M. F., and McDonald, N. Q. (2005) Structure of an XPF endonuclease with and without DNA suggests a model for substrate recognition. *EMBO J. 24*, 895−905.
(19) Chang, J. H., Kim, J. J., Choi, J. M., Lee, J. H., and Cho, Y. (2014) Crystal structure of the Mus81−Eme1 complex. *Genes Dev. 22*, 1093−1106.
(20) Hickman, A. B., Li, Y., Mathew, S. V., May, E. W., Craig, N. L., and Dyda, F. (2000) Unexpected structural diversity in DNA recombination: The restriction endonuclease connection. *Mol. Cell 5*, 1025−1034.
(21) Nishino, T., Komori, K., Tsuchiy, D., Ishino, Y., and Morikawa, K. (2001) Crystal structure of the archaeal Holliday junction resolvase Hjc and implications for DNA recognition. *Structure 9*, 197−204.
(22) Middleton, C. L., Parker, J. L., Richard, D. J., White, M. F., and Bond, C. S. (2004) Substrate recognition and catalysis by the Holliday junction resolving enzyme Hje. *Nucleic Acids Res. 32*, 5442−5451.
(23) Hadden, J. M., Déclais, A.-C., Phillips, S. E. V., and Lilley, D. M. J. (2002) Metal ions bound at the active site of the junction-resolving enzyme T7 endonuclease I. *EMBO J. 21*, 3505−3515.
(24) Hadden, J. M., Déclais, A.-C., Carr, S. B., Lilley, D. M. J., and Phillips, S. E. V. (2007) The structural basis of Holliday junction resolution by T7 endonuclease I. *Nature 449*, 621−624.
(25) Lemak, S., Beloglazova, N., Nocek, B., Skarina, T., Flick, R., Brown, G., et al. (2013) Toroidal structure and DNA cleavage by the CRISPR-associated [4Fe-4S] cluster containing Cas4 nuclease SSO0001 from *Sulfolobus solfataricus*. *J. Am. Chem. Soc. 135*, 17476−17487.
(26) Dias, A., Bouvier, D., Crépin, T., McCarthy, A. A., Hart, D. J., Baudin, F., et al. (2009) The cap-snatching endonuclease of influenza virus polymerase resides in the PA subunit. *Nature 458*, 914−918.
(27) Xiang, S., Cooper-Morgan, A., Jiao, X., Kiledjian, M., Manley, J. L., and Tong, L. (2009) Structure and function of the 5′-3′ exoribonuclease Rat1 and its activating partner Rai1. *Nature 458*, 784−788.
(28) Jiao, X., Chang, J. H., Kilic, T., Tong, L., and Kiledjian, M. (2013) A mammalian pre-mRNA 5′-end capping quality control mechanism and an unexpected link of capping to pre-mRNA processing. *Mol. Cell 50*, 104−115.
(29) Chang, J. H., Jiao, X., Chiba, K., Oh, C., Martin, C. E., Kiledjian, M., and Tong, L. (2012) Dxo1 is a new type of eukaryotic enzyme with both decapping and 5′-3′ exoribonuclease activity. *Nat. Struct. Mol. Biol. 19*, 1011−1017.
(30) Andreeva, A., Howorth, D., Candonia, J.-M., Brenner, S. E., Hubbard, T. J. P., Chothia, C., and Murzin, A. G. (2007) Data growth and its impact on the SCOP database: New developments. *Nucleic Acids Res. 36*, D419−D425.
(31) Steczkiewicz, K., Muszewska, A., Knizewski, L., Rychlewski, L., and Krzysztof, G. (2012) Sequence, structure and functional diversity of PD-(D/E)XK phosphodiesterase superfamily. *Nucleic Acids Res. 40*, 7016−7045.
(32) Laganeckas, M., Margelevicius, M., and Venclovas, C. (2010) Identification of new homomlogs of PD-(D/E)XK nucleases by support vector machines trained on data derived from profile-profile alignments. *Nucleic Acids Res. 39*, 1187−1196.
(33) Beese, L. S., and Steitz, T. A. (1991) Structural basis for the 3′-5′ exonuclease activity of *Escherichia coli* DNA polymerase I: A two metal ion mechanism. *EMBO J. 10*, 25−33.
(34) Yang, W., Lee, J. Y., and Nowotny, M. (2006) Making and breaking nucleic acids: Two-Mg^{2+}-ion catalysis and substrate specificity. *Mol. Cell 22*, 5−13.
(35) Nowotny, M., Gaidamakov, S. A., Crouch, R. J., and Yang, W. (2005) Crystal structures of RNase H bound to an RNA/DNA hybrid: Substrate specificity and metal-dependent catalysis. *Cell 121*, 1005−1016.
(36) Viadiu, H., and Aggarwal, A. K. (1998) The role of metals in catalysis by the restriction endonuclease *Bam*H1. *Nat. Struct. Biol. 5*, 910−916.
(37) Newman, M., Lunnen, K., Wilson, G., Greci, J., Schildkraut, I., and Phillips, S. E. V. (1998) Crystal structure of restriction endonuclease *Bgl*I bound to its interrupted DNA recognition sequence. *EMBO J. 17*, 5466−5467.
(38) Kaus-Drobek, M., Czapinska, H., Sokolowska, M., Tamulaitis, G., Szczepanowski, R. H., Urbanke, C., Siksnys, V., and Bochtler, M. (2007) Restriction endonuclease *Mva*I is a monomer that recognizes its target sequence asymmetrically. *Nucleic Acids Res. 35*, 2035−2046.
(39) Sokolowska, M., Kaus-Drobek, M., Czapinska, H., Tamulaitis, G., Szczepanowski, R. H., Urbanke, C., Siksnys, V., and Bochtler, M. (2007) Monomeric restriction endonuclease *Bcn*I in the apo form and in an asymmetric complex with target DNA. *J. Mol. Biol. 369*, 722−734.
(40) Zhang, J., McCabe, K. A., and Bell, C. E. (2011) Crystal structures of lambda exonuclease in complex with DNA suggest an electrostatic ratchet mechanism for processivity. *Proc. Natl. Acad. Sci. U.S.A. 108*, 11872−11877.
(41) Deibert, M., Grazulis, S., Sasnauskas, G., Siksnys, V., and Huber, R. (2000) Structure of the tetrameric restriction endonuclease *Ngo*MIV in complex with cleaved DNA. *Nat. Struct. Biol. 7*, 792−798.
(42) Etzkorn, C., and Horton, N. C. (2004) Mechanistic insights from the structures of *Hinc*II bound to cognate DNA cleaved from addition of Mg^{2+} and Mn^{2+}. *J. Mol. Biol. 343*, 833−849.
(43) Bauman, J. D., Patel, D., Baker, S. F., Vijayan, S. K., Xiang, A., Parhi, A. K., et al. (2013) Crystallographic fragment screening and structure-based optimization yields a new class of influenza endonuclease inhibitors. *ACS Chem. Biol. 8*, 2501−2508.
(44) Lukacs, C. M., Kucera, R., Schildkraut, I., and Aggarwal, A. K. (2000) Understanding the immutability of restriction enzymes: Crystal structure of *Bgl*II and its DNA substrate at 1.5 Å resolution. *Nat. Struct. Biol. 2*, 134−140.
(45) Etzkorn, C., and Horton, N. C. (2004) Ca^{2+} binding in the active site of *Hinc*II: Implications for the catalytic mechanism. *Biochemistry 43*, 13256−13270.
(46) Kostrewa, D., and Winkler, F. K. (1995) Mg^{2+} binding to the active site of *Eco*RV endonuclease: A crystallographic study of complexes with substrate and product DNA at 2 Å resolution. *Biochemistry 34*, 683−696.

(47) Grigorescu, A., Horvath, M., Wilkosz, P. A., Chandrasekhar, K., and Rosenberg, J. M. (2004) The integration of recognition and cleavage: X-ray structures of the pre-transition state complex, post-reactive complex, and the DNA-free endonuclease. In *Restriction Endonucleases* (Pingoud, A., Ed.) pp 137−177, Springer, Berlin.
(48) Horton, J. R., and Cheng, X. (2000) *Pvu*II endonuclease contains two calcium ions in active sites. *J. Mol. Biol. 300*, 1049−1056.
(49) Horton, N. C., and Perona, J. J. (2004) DNA cleavage by *Eco*RV endonuclease: Two metal ions in three metal ion-binding sites. *Biochemistry 43*, 6841−6857.
(50) Vipond, I. B., Baldwin, G. S., and Halford, S. E. (1995) Divalent metal ions at the active sites of the *Eco*RV and *Eco*RI restriction endonucleases. *Biochemistry 34*, 697−704.
(51) Groll, D. H., Jeltch, A., Selent, U., and Pingoud, A. (1997) Does the restriction endonuclease *Eco*RV employ a two-metal-ion mechanism for DNA cleavage? *Biochemistry 36*, 11389−11401.
(52) Baldwin, G. S., Sessions, R. B., Erskine, S. G., and Halford, S. E. (1999) DNA cleavage by the *Eco*RV restriction endonuclease: Roles of divalent metal ions in specificity and catalysis. *J. Mol. Biol. 288*, 87−103.
(53) Pingoud, V., Wende, W., Friedhoff, P., Reuter, M., Alves, J., Jeltsch, A., et al. (2009) On the divalent metal ion dependence of DNA cleavage by restriction endonucleases of the *Eco*RI family. *J. Mol. Biol. 393*, 140−160.
(54) Strong, M., Sawaya, M. R., Wang, S., Phillips, M., Cascio, D., and Eisenberg, D. (2006) Toward the structural genomics of complexes: Crystal structure of a PE/PPE protein complex from *Mycobacterium tuberculosis*. *Proc. Natl. Acad. Sci. U.S.A. 103*, 8060−8065.
(55) Collaborative Computational Project, Number 4 (1994) The CCP4 Suite: Programs for protein crystallography. *Acta Crystallogr. D50*, 760−763.
(56) Emsley, P., Lohkamp, B., Scott, W. G., and Cowtan, K. (2010) Features and development of Coot. *Acta Crystallogr. D66*, 486−501.
(57) *The PyMOL Molecular Graphics System*, version 0.99; Schrödinger, LLC, Portland, OR.
(58) Jeltsch, A., Alves, J., Maass, G., and Pingoud, A. (1992) On the catalytic mechanism of *Eco*RI and *Eco*RV. A detailed proposal based on biochemical results, structural data and molecular modeling. *FEBS Lett. 304*, 4−8.
(59) Jeltsch, A., Alves, J., Wolfes, H., Maass, G., and Pingoud, A. (1993) Substrate-assisted catalysis in the cleavage of DNA by the *Eco*RI and *Eco*RV restriction enzymes. *Proc. Natl. Acad. Sci. U.S.A. 90*, 8499−8503.
(60) Jeltsch, A., Pleckaityte, M., Selent, U., Wolfes, H., Siksnys, V., and Pingoud, A. (1995) Evidence for substrate-assisted catalysis in the DNA cleavage of several restriction endonucleases. *Gene 157*, 157−162.
(61) Koziolkiewicz, M., and Stec, W. J. (1992) Application of phosphate-backbone-modified oligonucleotides in the studies on *Eco*RI endonuclease mechanism of action. *Biochemistry 31*, 9460−9466.
(62) Thorogood, H., Grasby, J. A., and Connolly, B. A. (1996) Influence of the phosphate backbone on the recognition and hydrolysis of DNA by the EcoRV restriction endonuclease. A study using oligodeoxynucleotide phosphorothioates. *J. Biol. Chem. 271*, 8855−8862.